Spectrally-resolved fluorescence cross sections of aerosolized biological live agents and simulants using five excitation wavelengths in a BSL-3 laboratory

Yong-Le Pan,[1,*] Steven C. Hill,[1] Joshua L. Santarpia,[2,4] Kelly Brinkley,[2] Todd Sickler,[3] Mark Coleman,[1] Chatt Williamson,[1] Kris Gurton,[1] Melvin Felton,[1] Ronald G. Pinnick,[1] Neal Baker,[2] Jonathan Eshbaugh,[2] Jerry Hahn,[2] Emily Smith,[2] Ben Alvarez,[2] Amber Prugh,[3] and Warren Gardner[3]

[1]*US Army Research Laboratory, 2800 Powder Mill Road, Adelphi, Maryland 20783, USA*
[2]*Johns Hopkins University, Applied Physics Laboratory, 11100 Johns Hopkins Road, Laurel, MD 20723, USA*
[3]*Edgewood Chemical and Biological Center, 5183 Blackhawk RD, APG, MD 21010, USA*
[4]*Present affiliation: Sandia National Laboratories, 1515 Eubank SE, Albuquerque, NM, 87123, USA*
[*]*yongle.pan.civ@mail.mil*

Abstract: A system for measuring spectrally-resolved fluorescence cross sections of single bioaerosol particles has been developed and employed in a biological safety level 3 (BSL-3) facility at Edgewood Chemical and Biological Center (ECBC). It is used to aerosolize the slurry or solution of live agents and surrogates into dried micron-size particles, and to measure the fluorescence spectra and sizes of the particles one at a time. Spectrally-resolved fluorescence cross sections were measured for (1) bacterial spores: *Bacillus anthracis* Ames (BaA), *B. atrophaeus* var. *globigii* (BG) (formerly known as *Bacillus globigii)*, *B. thuringiensis israelensis* (Bti), *B. thuringiensis kurstaki (*Btk), *B. anthracis* Sterne (BaS); (2) vegetative bacteria: *Escherichia coli (E. coli)*, *Pantoea agglomerans* (Eh) (formerly known as *Erwinia herbicola*), *Yersinia rohdei* (Yr), *Yersinia pestis CO92* (Yp); and (3) virus preparations: *Venezuelan equine encephalitis TC83* (VEE) and the bacteriophage *MS2*. The excitation wavelengths were 266 nm, 273 nm, 280 nm, 365 nm and 405 nm.

OCIS codes: (280.1415) Biological sensing and sensors; (010.1100) Aerosol detection; (300.2530) Fluorescence, laser-induced; (300.6280) Spectroscopy, fluorescence and luminescence; (120.6200) Spectrometers and spectroscopic instrumentation.

References and links

1. A. Fernstrom and M. Goldblatt, "Aerobiology and its role in the transmission of infectious disease," J. Pathogens **2013**, 1–13 (2013).
2. Y. L. Pan, J. D. Eversole, P. Kaye, V. Foote, R. G. Pinnick, S. C. Hill, M. W. Mayo, and R. K. Chang, "Bio-aerosol fluorescence," in *Optics of Biological Particles (NATO Science Series II: Mathematics Physics and Chemistry)*, A. Hoekstra, V Maltsev, and G Videen, eds., (Springer, 2006), pp. 63–164.
3. P. P. Hairston, J. Ho, and F. R. Quant, "Design of an instrument for real-time detection of bioaerosols using simultaneous measurement of particle aerodynamic size and intrinsic fluorescence," J. Aerosol Sci. **28**(3), 471–482 (1997).
4. F. L. Reyes, T. H. Jeys, N. R. Newbury, C. A. Primmerman, G. S. Rowe, and A. Sanchez, "Bio-aerosol fluorescence sensor," Field Anal. Chem. Technol. **3**(4–5), 240–248 (1999).
5. M. Seaver, J. D. Eversole, J. J. Hardgrove, W. K. Cary, Jr., and D. C. Roselle, "Size and fluorescence measurements for field detection of biological aerosols," Aerosol Sci. Technol. **30**(2), 174–185 (1999).
6. V. Sivaprakasam, H. B. Lin, A. L. Huston, and J. D. Eversole, "Spectral characterization of biological aerosol particles using two-wavelength excited laser-induced fluorescence and elastic scattering measurements," Opt. Express **19**(7), 6191–6208 (2011).
7. P. H. Kaye, W. R. Stanley, E. Hirst, E. V. Foot, K. L. Baxter, and S. J. Barrington, "Single particle multichannel bio-aerosol fluorescence sensor," Opt. Express **13**(10), 3583–3593 (2005).

#199333 - $15.00 USD Received 14 Oct 2013; revised 21 Feb 2014; accepted 26 Feb 2014; published 1 Apr 2014

8. K. L. Schroder, P. J. Hargis, Jr., R. L. Schmitt, D. J. Rader, and I. R. Shokair, "Development of an unattended ground sensor for ultraviolet laser-induced fluorescence detection of biological agent aerosols," Proc. SPIE **3855**, 82–91 (1999).
9. J. A. Huffman, B. Treutlein, and U. Pöschl, "Fluorescent biological aerosol particle concentrations and size distributions measured with an Ultraviolet Aerodynamic Particle Sizer (UV-APS) in Central Europe," Atmos. Chem. Phys. **10**(7), 3215–3233 (2010).
10. D. Kiselev, L. Bonacina, and J.-P. Wolf, "A flash-lamp based device for fluorescence detection and identification of individual pollen grains," Rev. Sci. Instrum. **84**(3), 033302 (2013).
11. Y. L. Pan, S. Holler, R. K. Chang, S. Hill, R. G. Pinnick, S. Niles, and J. R. Bottiger, "Single-shot fluorescence spectra of individual micrometer-sized bioaerosols illuminated by a 351- or a 266-nm ultraviolet laser," Opt. Lett. **24**(2), 116–118 (1999).
12. S. C. Hill, R. G. Pinnick, S. Niles, Y. L. Pan, S. Holler, R. K. Chang, J. R. Bottiger, B. T. Chen, C. S. Orr, and G. Feather, "Real-time measurement of fluorescence spectra from single airborne biological particles," Field Anal. Chem. Technol. **3**(4–5), 221–239 (1999).
13. Y. L. Pan, R. G. Pinnick, S. C. Hill, J. M. Rosen, and R. K. Chang, "Single-particle laser-induced-fluorescence spectra of biological and other organic-carbon aerosols in the atmosphere: Measurements at New Haven, Connecticut, and Las Cruces, New Mexico," J. Geophys. Res. **112**, D24S19 (2007).
14. Y. L. Pan, S. C. Hill, R. G. Pinnick, H. Huang, J. R. Bottiger, and R. K. Chang, "Fluorescence spectra of atmospheric aerosol particles measured using one or two excitation wavelengths: Comparison of classification schemes employing different emission and scattering results," Opt. Express **18**(12), 12436–12457 (2010).
15. R. Bhartia, W. F. Hug, E. C. Salas, R. D. Reid, K. K. Sijapati, A. Tsapin, W. Abbey, K. H. Nealson, A. L. Lane, and P. G. Conrad, "Classification of organic and biological materials with deep ultraviolet excitation," Appl. Spectrosc. **62**(10), 1070–1077 (2008).
16. J. R. Lakowicz, *Principles of Fluorescence Spectroscopy* (Plenum, 1983), pp. 341–343.
17. A. Manninen, M. Putkiranta, J. Saarela, A. Rostedt, T. Sorvajärvi, J. Toivonen, M. Marjamäki, J. Keskinen, and R. Hernberg, "Fluorescence cross sections of bioaerosols and suspended biological agents," Appl. Opt. **48**(22), 4320–4328 (2009).
18. C. Pöhlker, J. A. Huffman, and U. Pöschl, "Autofluorescence of atmospheric bioaerosols – fluorescent biomolecules and potential interferences," Atmos. Meas. Tech. **5**(1), 37–71 (2012).
19. D. E. Wilson, and L.C. Chosewood, eds., *Biosafety in Microbiological and Biomedical Laboratories (BMBL)*, 5th ed. (US Dept. Health and Human Services, 2009).
20. K. Rhodes, "High-containment biosafety laboratories, Preliminary observations on the oversight of the Proliferation of BSL-3 and BSL-4 laboratories in the United States," GAO-08–108T. Testimony before the Subcomittee on Oversight and Investigations (2007), p. 10.
21. H. U. Kim and J. M. Goepfert, "A sporulation medium for Bacillus anthracis," J. Appl. Bacteriol. **37**(2), 265–267 (1974).
22. L. A. Mattieson and J. L. Saunderson, "Optical and electrical properties of polystyrenes," in *Styrene: its Polymers, Copolymers and Derivatives*, R. H. Boundy, R. F. Boyer, and S. M. Stoesser, eds. (Reinhold, 1952), p. 524.
23. T. Inagaki, E. T. Arakawa, R. N. Hamm, and M. W. Williams, "Optical properties of polystyrene from the near-infrared to the X-ray region and convergence of optical sum rules," Phys. Rev. B **15**(6), 3243–3253 (1977).
24. P. W. Barber and S. C. Hill, *Light Scattering by Particles: Computational Methods* (World Scientific, 1990).
25. S. C. Hill, V. Boutou, J. Yu, S. Ramstein, J. P. Wolf, Y. Pan, S. Holler, and R. K. Chang, "Enhanced backward-directed multiphoton-excited fluorescence from dielectric microcavities," Phys. Rev. Lett. **85**(1), 54–57 (2000).
26. Y. L. Pan, S. C. Hill, J. P. Wolf, S. Holler, R. K. Chang, and J. R. Bottiger, "Backward-enhanced fluorescence from clusters of microspheres and particles of tryptophan," Appl. Opt. **41**(15), 2994–2999 (2002).
27. J. L. Santarpia, Y. L. Pan, S. C. Hill, N. Baker, B. Cottrell, L. McKee, S. Ratnesar-Shumate, and R. G. Pinnick, "Changes in fluorescence spectra of bioaerosols exposed to ozone in a laboratory reaction chamber to simulate atmospheric aging," Opt. Express **20**(28), 29867–29881 (2012).
28. G. W. Faris, A. Williams, C. B. Carlisle, and B. V. Bronk, "Spectrally resolved absolute fluorescence cross sections of B. Globigii and B. Cereus," SRI technical Note, SRI project 2913 (May 1992).
29. G. W. Faris, R. A. Copeland, K. Mortelmans, and B. V. Bronk, "Spectrally resolved absolute fluorescence cross sections for bacillus spores," Appl. Opt. **36**(4), 958–967 (1997).
30. V. Sivaprakasam, A. Huston, C. Scotto, and J. Eversole, "Multiple UV wavelength excitation and fluorescence of bioaerosols," Opt. Express **12**(19), 4457–4466 (2004).
31. J. Kunnil, S. Sarasanandarajah, E. Chacko, and L. Reinisch, "Fluorescence quantum efficiency of dry Bacillus globigii spores," Opt. Express **13**(22), 8969–8979 (2005).
32. J. R. Stephens, "Measurements of the ultraviolet fluorescence cross sections and spectra of bacillus anthracis simulants," Los Alamos National Lab Report, LAUR-98–4173 (May, 1999).
33. J. Atkins, M. E. Thomas, and R. I. Joseph, "Spectrally resolved fluorescence cross sections of BG and BT with a 266-nm pump wavelength," Proc. SPIE **6554**, 65540T1 (2007).
34. R. Weichert, W. Klemm, K. Legenhausen, and C. Pawellek, "Determination of fluorescence cross-sections of biological aerosols," Part. Part. Syst. Charact. **19**(3), 216–222 (2002).
35. M. Carrera, R. O. Zandomeni, J. Fitzgibbon, and J. L. Sagripanti, "Difference between the spore sizes of Bacillus anthracis and other Bacillus species," J. Appl. Microbiol. **102**(2), 303–312 (2007).

#199333 - $15.00 USD Received 14 Oct 2013; revised 21 Feb 2014; accepted 26 Feb 2014; published 1 Apr 2014

36. C. Laflamme, J.-R. Simard, S. Buteau, P. Lahaie, D. Nadeau, B. Déry, O. Houle, P. Mathieu, G. Roy, J. Ho, and C. Duchaine, "Effect of growth media and washing on the spectral signatures of aerosolized biological simulants," Appl. Opt. **50**(6), 788–796 (2011).
37. J.-R. Simard, G. Roy, P. Mathieu, V. Larochelle, J. McFee, and J. Ho, "Standoff sensing of bioaerosols using intensified range-gated spectral analysis of laser-induced fluorescence," IEEE Trans. Geosci. Remote Sens. **42**(4), 865–874 (2004).
38. B. Dery, S. Buteau, J.-R. Simard, J.-P. Bouchard, and R. Vallee, "Spectroscopic calibration correlation of field and lab-sized fluorescence lidar systems," IEEE Trans. Geosci. Remote Sens. **48**(9), 3580–3586 (2010).
39. G. Mejean, J. Kasparian, J. Yu, S. Frey, E. Salmon, and J.-P. Wolf, "Remote detection and identification of biological aerosols using a femtosecond terawatt lidar system," Appl. Phys. B **78**, 535–537 (2004).
40. A. Rondi, D. Kiselev, S. Machado, J. Extermann, S. Weber, L. Bonacina, J. P. Wolf, J. Roslund, M. Roth, and H. Rabitz, "Discriminating biomolecules with coherent control strategies," Chimia (Aarau) **65**(5), 346–349 (2011).

1. Introduction

Many infectious diseases of humans, animals, and plants are transmitted by airborne microorganisms in droplets or particles [1]. Human diseases transmissible by aerosol particles include some of those carried by bacteria (e.g., tuberculosis, several pneumonias, Legionellosis, Q fever, and anthrax); viruses (e.g., influenza, several pneumonias, severe acute respiratory syndrome (SARS), chicken pox, measles, hanta fever); and fungi (e.g., histoplasmosis, several pneumonias). Airborne transmission of prions has also been suggested to occur in humans. Asthma and other allergies of the respiratory tract can be caused by airborne pollens, proteins (e.g., those in the dried saliva of cats), fungal spores, insect parts or droppings, etc. Identification of specific microorganisms in aerosol particles requires culturing (which may take a week or more) or analysis of the particles for specific antigens or sequences of nucleic acids (which requires reagents and may take a few minutes to days). There is interest in reagentless monitors for harmful bioaerosols that run continuously with little maintenance and rapidly provide an indication of the presence of threat particles. Although such monitors are not sufficiently specific to identify particular organisms, they could indicate changes in concentrations of total aerosols, or of aerosols in particular categories (e.g., bacteria-like), they could indicate when to turn on instruments which identify specific microorganisms. Depending on the circumstances, the readings from these rapid, reagentless monitors might be used in making immediate decisions about protecting people from hazardous aerosols. Although the largest impetus for developing rapid reagentless detectors for bioaerosols may arise from the desire to detect bioterrorism/biowarfare agents, the need for rapid reagentless detection of other communicable airborne microorganisms (e.g., tuberculosis, SARS, influenza viruses) is also large.

A variety of reagentless methods have been studied and/or used for real-time detection and characterization of aerosols, especially bioaerosol particles [2–15]. They are mainly based on the measurements of elastic scattering, fluorescence, laser induced breakdown spectroscopy (LIBS), or mass spectroscopy of individual aerosol particles [2]. Fluorescence-based systems have been developed by several groups [e.g 3–15]. These systems, typically combined with measurements of elastic scattering from each particle to estimate particle size, are employed in most of the biological-agent point-sensor early warning systems. Such systems have been used to study the fluorescence of bioaerosols and other fluorescent particles in the laboratory [e.g., 10–12, 16–18], and to make continuous reagentless fluorescence measurements of atmospheric aerosols on several continents [e.g 5, 9, 13–15]. The commercial availability [2] and relatively low cost make feasible the deployment of such instruments for routine continuous monitoring. However, the development and initial testing of these systems (including their detection algorithms) for infectious agents is often done with simulants or, less commonly, with killed agents. For example, *B. subtilis* and *B. thuringiensis kurstaki* are often used as simulants for *B. anthracis*. Some questions regarding agents and simulants are as follows. 1) For any given live agent and simulant pair, does the live agent have the same detection-relevant properties as the simulant? In the case of fluorescence detection systems, spectrally resolved fluorescence cross sections at the relevant excitation

#199333 - $15.00 USD Received 14 Oct 2013; revised 21 Feb 2014; accepted 26 Feb 2014; published 1 Apr 2014

wavelengths would be the most important properties. 2) Do the relevant properties of agents and simulants change in the same way after they are aerosolized, released into the atmosphere, and subjected to sunlight, water vapor, and reactive molecules such as ozone and hydroxyl radicals? Answering these and similar questions requires the development of BSL-3 systems in which aerosols from simulants and live agents can be generated and their relevant properties can be measured and compared.

Biosafety Level 3 (BSL-3) guidelines specify the requirements for working with BSL-3 agents, i.e., "indigenous or exotic agents that may cause serious or potentially lethal disease through the inhalation route of exposure" [19] but for which treatments are available, e.g., tuberculosis, SARS, and anthrax. Lethal agents that can be transmitted as aerosols, but which have no treatment available (e.g., Ebola), are classed as BSL-4. In the primary document used in the United States for procedures and policies for handling bioagents, i.e., Biosafety in Microbiological and Biomedical Laboratories 5 (BMBL5), all microorganisms are termed "agents" [19]. For example, BSL-1 agents are "agents that are not known to cause disease in normal healthy humans." However, in this paper the term "agent" with no adjective refers to agents that require handling under BSL-3 procedures. This group includes the most of the biowarfare/bioterrorism agents. In 2007 there were 1356 BSL-3 laboratories [20] (1042 registered with the US Center for Disease Control (CDC) and 314 registered with the US Dept. of Agriculture). In most work done in BSL-3 laboratories, the microorganisms are not intentionally aerosolized. Aerosolization of agents requires higher degrees of protection.

This paper reports the development of a system that can: a) generate single aerosol-particles composed of agents or simulants using a Sono-Tek ultrasonic nozzle; b) measure their single-particle fluorescence spectra using a modified single-particle fluorescence spectrometer (SPFS) [e.g 13] using a wavelength tunable, fire-on-demand laser; c) measure the near-forward elastic scattering to estimate the particle size; and d) measure the size distribution, concentration, and average fluorescence per particle at each size bin (using the TSI UV-APS). The system can illuminate the particles at many different wavelengths from 220 to 450 nm. It was assembled and used at the BSL-3 facility at Edgewood Chemical and Biological Center (ECBC).

The goal of this system was to measure single-particle fluorescence properties of aerosols excited at five different wavelengths. No stand-alone, remotely operated system was available to make these measurements. One major difficulty was that no equipment that was potentially exposed to live agents could be removed for later use outside of the BSL-3 lab. In the case of these fluorescence measurements, much of the required equipment is expensive, and could be damaged by the vaporous hydrogen peroxide used for decontamination. Therefore, the tunable laser system, much of the electronics for the detection and controlling equipments, and the system operators stayed outside of the BSL-3 laboratory. A second problem is that even if, e.g., a sacrificial, tunable, pulse-on-demand laser, were placed within the BSL-3 room, it would be unmanageable for the BSL-3 certified personnel in the necessary personal protective equipment (PPE) to change the wavelengths and do the required realignment for multiple wavelength excitation. A third problem is that the total number of personnel that work inside the BSL-3 room have to be minimized. Therefore, the system was designed so that all personnel required for data acquisition and instrument control would work from outside of the BSL-3 room, and only a limited amount of equipments would be installed within the BSL-3 chamber and would be remotely controlled.

This paper also describes the calibration of the system and reports the fluorescence spectral profiles and fluorescence cross sections from aerosolized live agents and simulants. These measured samples include: (1) bacterial spores, i.e., *B. anthracis* Ames (BaA), *B. anthracis* Sterne (BaS), *B. atrophaeus* var. *globigii* (BG) (*formerly Bacillus globigii*), *B. thuringiensis israelensis* (Bti), *Bacillus thuringiensis kurstaki (*Btk); (2) vegetative bacteria, i.e., *Escherichia coli (E. coli), Pantoea agglomerans (formerly Erwinia herbicola*; Eh), *Yersinia rohdei* (Yr), *Yersinia pestis CO92* (Yp); and (3) viruses, i.e., MS2 (a bacteriophage)

#199333 - $15.00 USD Received 14 Oct 2013; revised 21 Feb 2014; accepted 26 Feb 2014; published 1 Apr 2014

and *Venezuelan equine encephalitis TC83* (VEE), where the virus-containing samples were primarily the lysate of the cells in which they were grown, along with spent culture media. Spectral measurements of BaS were made from three different preparations. Five wavelengths (266, 273, 280, 365, and 405 nm) from the laser system were selected for fluorescence excitation.

2. System development and arrangement

The system was set up in the ECBC BSL-3 laboratory, which is located on Aberdeen Proving Ground (APG), MD, USA. One of the design requirements was to prevent aerosolized agent from coming into contact with persons or being released into the environment. To meet this requirement, four layered regions of confinement, each with a lower pressure, were used. The BSL-3 chamber is a stainless steel glovebox. It is kept under constant negative pressure with respect to the BSL-3 room, which is kept under constant negative pressure with respect to the hallway and atmospheric air. The air pressures are controlled by a dedicated HEPA-filtered supply/exhaust air handling system. The pumps for the air handling system are on an emergency generator backup system. Only authorized, trained personnel wearing Tyvek suits with powered air-purifying respirators can enter the BSL-3 rooms.

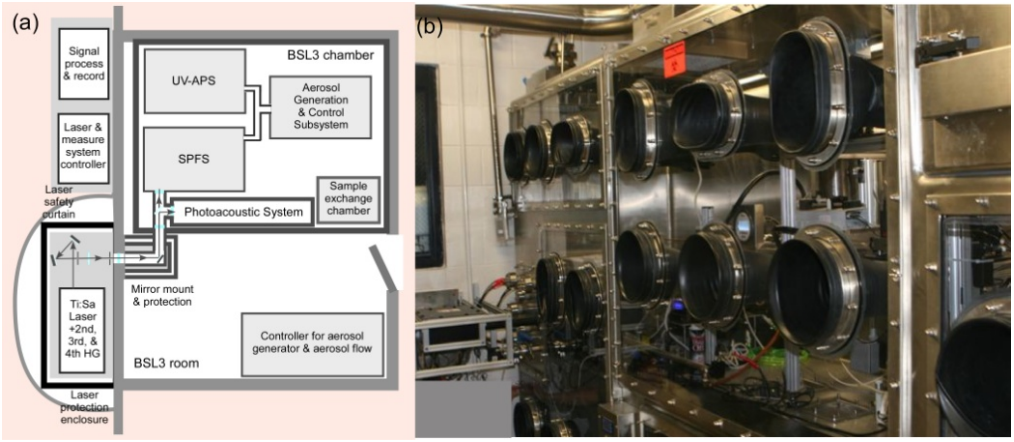

Fig. 1. (a) Schematic of the system at the ECBC BSL-3 facility for measuring spectrally resolved fluorescence cross sections of aerosolized live agents and surrogates; (b) Photograph of the BSL-3 chamber (i.e., the glovebox) within the BSL-3 room. Also visible on the far left is the enclosure for the laser beam as it enters the room and the mirror that directs the beam.

Figure 1(a) shows the system arrangement in the BSL-3 facility. The system includes components positioned outside the BSL-3 chamber (in the adjacent hallway), as well as components inside the BSL-3 room and chamber. Figure 1(b) presents a photo of the BSL-3 chamber with a mirror mount (on the wall at left) and parts of the installed system inside of the BSL-3 chamber.

Components of the system include: (1) the excitation laser subsystem; (2) the instrument controller and data acquisition subsystem; (3) the aerosol generation and control subsystem; (4) the single particle fluorescence spectrometer (SPFS) subsystem; and (5) an ultraviolet aerodynamic particle sizer (UV-APS). Subsystems (1) and (2) are located outside the BSL-3 room in the hallway. Subsystems (3)-(5) are located inside of the BSL-3 chamber, although some of the electronics, such as hardware controller and the data acquisition instruments for the fluorescence spectra are in the hallway. To pass cables between the BSL-3 room and BSL-3 chamber, standard vacuum electronic feedthroughs are used. These cables are used for controlling the filter wheel, fine adjustments of the aerosol nozzle etc., and for signal and data communications. The details of each subsystem will be described below.

#199333 - $15.00 USD Received 14 Oct 2013; revised 21 Feb 2014; accepted 26 Feb 2014; published 1 Apr 2014

To minimize the possibility of the aerosolized live agents coming in contact with any persons, inside the BSL-3 room or outside, the air pressure within the aerosol generation and control subsystem is negative with respect that in the BSL-3 chamber. The air pressure in the SPFS and the UV-APS sample regions is also negative with respect to that in the aerosol generation and control subsystem. This is illustrated in more detail below under Section 2.3 on the aerosol generation and control subsystem.

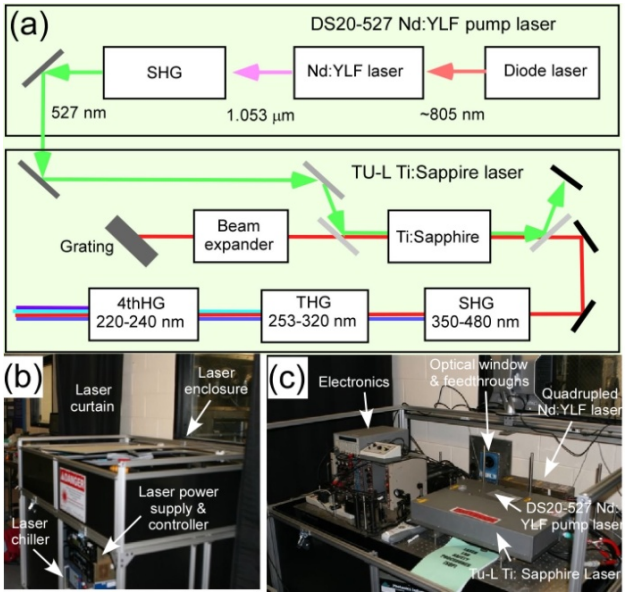

Fig. 2. (a) Diagram of the excitation laser (Photonics Industries, TU-L 10-291 laser with DS20-527 pump laser); (b) Photograph of the enclosure for the laser. The laser power supply and controller, as well as the cooling system are under the optical table. (c) The laser on the optical table in the hallway, with protective enclosure removed. On the right, closest to the observer, is the laser head of the Ti:Sapphire laser with its SHG, THG, & 4thHG. Behind it on the right is the head for the DS20-527 pump laser, and behind that is another frequency quadrupled Nd:YLF laser which was used for reference alignment. On the left of the optical table is some electronics for controlling the laser and for processing the signals from the photomultipliers (PMTs) which are used to determine when a particle is about to enter the sample volume of the SPFS. The window that allows the laser beam to pass from the hallway into the BSL-3 room is visible in a blue Roxtex material.

2.1 The excitation laser subsystem

Figure 2 shows a narrow band (< 3 GHz), tunable (200–450 nm), Q-switched, triggerable on-demand (1Hz–4 kHz), diode-laser-pumped solid state (DPSS) Ti:Sapphire laser system with its 2nd- 3rd- and 4th-harmonic generation (SHG, THG, and 4thHG). The pulse duration is within 10–30 ns (depending on wavelength, current, and repetition rate), and the pulse energy is larger than 50 μJ/pulse when triggered below 1 KHz at all the wavelengths used in this study.

To protect personnel from exposure to laser emission, and to protect the laser from being bumped, which may cause instability or misalignment, an aluminum-framed enclosure with removable top and side covers was built. It was installed against the hallway wall surrounding the laser optical table, with a 1-inch gap between the optical table and the enclosure. During laser operation, the enclosure was totally closed to block any leakage of the laser beam (direct or scattered). During the alignment period, the top cover was removed and the entire system was enclosed by a laser curtain in the hallway (see Fig. 1). The laser could be turned on only when either (or both) the enclosure interlock or the curtain interlock was secured.

#199333 - $15.00 USD Received 14 Oct 2013; revised 21 Feb 2014; accepted 26 Feb 2014; published 1 Apr 2014

The excitation wavelengths, 266 nm, 273 nm, 280 nm, 365 nm, and 405 nm were chosen to match the most popular excitation wavelengths used in existing or contemplated fluorescence-based bioaerosol detection systems. The laser outputs at 266 nm, 273 nm, and 280 nm are from the THG of the Ti:Sapphire laser. The laser outputs at 365 nm and 405 nm are from the SHG.

The laser-beam propagation direction is slightly different for each wavelength, each of which requires different angles of the HG crystals. These angles are adjusted for phase matching. Several times per year the BSL-3 laboratory is decontaminated and agent materials are secured so that work may be done in the laboratory without significant PPE. During this period, we were allowed to enter the BSL-3 room and open the BSL-3 chamber to adjust the system to make sure that the pulses of the laser beam could illuminate the particles at the right position within the sampling volume. However, as soon as agents were once again in use, the glovebox would remain closed for months. Further alignment of the laser beam within the BSL-3 room was impossible. Even if the system had been perfectly aligned at one particular wavelength, it would become misaligned when the laser was tuned to a new wavelength. Each time the wavelength was changed, the laser beam had to be repositioned so that it illuminated the particles in the center of the sample volume. The laser beam diameter was about 1 mm.

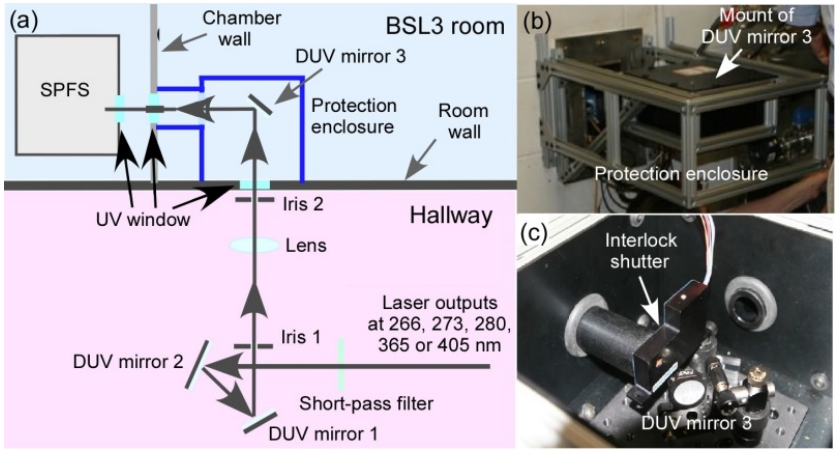

Fig. 3. (a) Schematic of the optical arrangement that provides for alignment of different wavelength laser beams so that they can interrogate individual particles in the aerosol jet at the right position in the sample volume within the SPFS inside of the BSL-3 chamber. (b) Photograph of the mount for deep ultra-violet (DUV) mirror 3 and the protective enclosure. (c) Photograph of the interlock shutter and DUV mirror 3 with its mount for steering the laser beam into the BSL-3 chamber.

Figure 3(a) shows the optical arrangement that enables realignment of the system to position different wavelength laser beams along the same propagation path, so that single particles can be reliably interrogated. Two irises are set about 0.6 m apart on the optical table in the hallway, outside the BSL-3 chamber. These irises define a beam path that is determined by the first aligned wavelength (273 nm here). Once the laser is tuned to another wavelength, two deep ultra-violet mirrors (DUV 1 and 2) are adjusted so that the laser beam can be realigned to propagate through the two irises and realign again. Fine adjustment to optimize the alignment is done by adjusting mirrors DUV 1 and DUV 2 to maximize the elastic scattering signal from test particles excited by the new-wavelength beam.

Alignment of the system would be less complicated if there were an optical fiber that could conduct sufficient energy over the 2 meters needed to reach the particle at wavelengths within the range (260–410 nm) used here. However, we cannot find any fiber that can transmit adequate energy to the particles, so the laser beam was arranged to propagate in free space as shown in Fig. 3. Here, the laser, deep UV mirror (DUV 3), and SPFS are on three

#199333 - $15.00 USD Received 14 Oct 2013; revised 21 Feb 2014; accepted 26 Feb 2014; published 1 Apr 2014

independent platforms. Movement of any one of them might result in misalignment of the system. In order to reduce the possibility of such a misalignment, the mirror mount was attached to the wall. A protective enclosure surrounding the mirror (Fig. 3(b)) was added to reduce the possibility of accidentally touching the mirror mount. The laser beam was totally covered by this enclosure and aluminum tubes. One interlock was also set to automatically block the laser in case someone accidently opened the enclosure inside the BSL-3 room (Fig. 3(c)).

2.2 The instrument control and data acquisition subsystem

Most of the controlling, data acquisition, processing, and recording subsystems are set up outside of the BSL-3 lab as shown in Fig. 4. Standard vacuum electronic feedthroughs were used to connect the cables through the BSL-3 chamber and BSL-3 room as shown in Figs. 4(b) and 4(c). These cables were used for system controlling, signal, and data communications. The connection and feedthrough panel included 25-pin and 12-pin D-type, 4-pin BNC-coaxial, USB feedthroughs between the BSL-3 chamber and the BSL-3 room (MDC corp., Fig. 4(b)); Roxtec pass-throughs were used between the BSL-3 room and the outside hallway (Fig. 4(c)), in which a wedge was used to press the rubber between the wall and cables. One ethernet cable, two USB cables, one RS232 cable, 12 BNC-coaxial cables, and five audio cables were used for analog and digital signal communication. Regular 120 V, 60 Hz power was supplied inside the BSL-3 chamber, BSL-3 room, and in the hallway. Other details are described in Section 2.4.

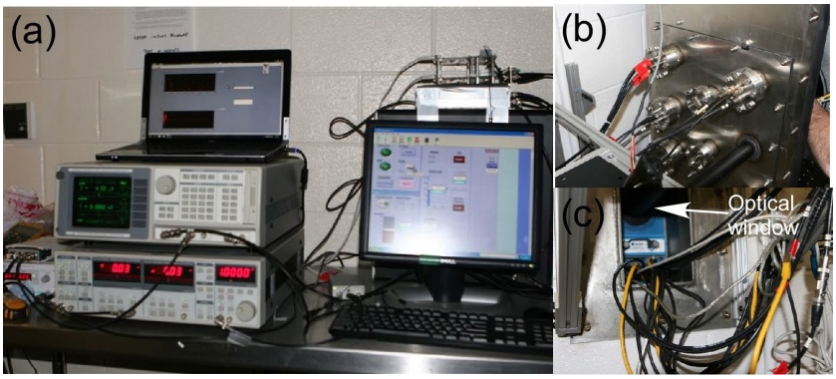

Fig. 4. Photographs of some of the (a) controllers, data acquisition, processing and recording electronics in the hallway; (b) electronic feedthroughs on the front panel of the BSL-3 chamber; and (c) electronic feedthroughs on the wall of the BSL-3 room; note the 2-in diameter fused silicon window at the top of the photo is for the laser beam.

2.3 Aerosol generation and control subsystem

The aerosol generation and control system (Fig. 5) was designed to provide controllable and consistent delivery of agent aerosols generated from their corresponding slurries or solutions, while also maintaining aerosol containment in both the generation and measurement regions of the system. The air pressure within the aerosol generation and control subsystem is negative with respect to that in the BSL-3 chamber. The air pressure in the SPFS and the UV-APS sample regions is negative with respect to that in the aerosol generation and control subsystem. The pressure difference at each stage is at least 0.1-0.5 inch H_2O, or greater.

#199333 - $15.00 USD Received 14 Oct 2013; revised 21 Feb 2014; accepted 26 Feb 2014; published 1 Apr 2014

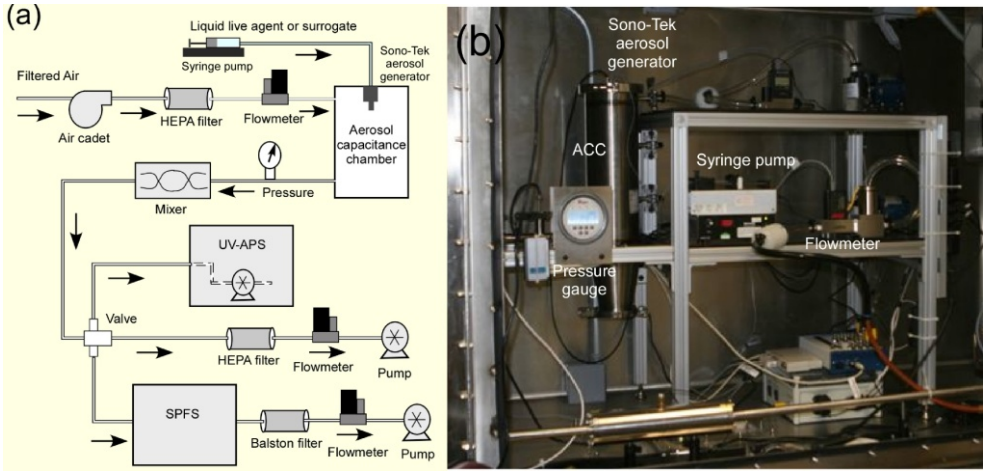

Fig. 5. (a) Schematic flow diagram of the aerosol generation and control system and the flow through the whole system within the BSL-3 chamber; (b) Photograph of the aerosol generation system within the BSL-3 chamber before the front panel is closed.

The system is designed as a "push/pull" system to provide better control of airflow rates through the system, and to help provide the ability to maintain the desired negative pressure regions while BSL-3 aerosols are in the system. The flowmeter/controller upstream from the aerosol capacitance chamber (ACC; Fig. 5(a)) controls the airflow rate. Aerosol is generated using a Sono-Tek ultrasonic spray nozzle, with 3-, 5-, 10- or 30-ml syringes. The nozzle used is chosen depending on the available slurry concentrations and amounts and the desired aerosol concentration and particle size. The pump infuses the liquid suspensions at rates between 1 and 100 μL/min (depending on the desired aerosol concentration). The ultrasonic nozzle is set to 3 W throughout all experiments. The nozzle of the Sono-Tek is oriented downward into the ACC. The ACC provides a way to dry the aerosol before it enters the mixing and measurement regions of the system. The air flowing into and through the ACC is controlled by a pressure regulator. The air flows through a turbidity mixer to help prevent "layering" of the aerosol-laden flow and clean air. The mixed air is then distributed to the SPFS (controlled to 1.0 Lpm by the flowmeter/controller downstream of the SPFS) and the UV-APS (controlled to 1.0 Lpm by internal flow control). The system is maintained at a desired negative pressure by using the pressure measurement to adjust the upstream flow and was kept to 0.5 inch H_2O (~1.25 mbar) for these experiments. The different agent and simulant aerosols are generated using this system. When switching between one agent or stimulant aerosol and the next, HEPA filtered air is continuously flowed through the system until no particle counts are observed on the UV-APS for an entire 10 s measurement period. In this way, the amount of contamination from one aerosol type to the next was minimized.

2.4 Single-particle fluorescence spectrometer (SPFS) subsystem

The single-particle fluorescence spectrometer (SPFS) subsystem is similar to those described previously [13] except that it: (a) does not include the particle concentrator; (b) added a 705-nm diode laser beam and PMT detector for estimating single particle size from the forward scatter; (c) has an additional PMT to record the shot-to-shot intensity of the laser pulse; (d) has a remote controllable filter wheel with filters for 5 different wavelengths to block the corresponding elastic scattering from entering the spectrometer; (e) has some expensive components packaged into different airtight boxes (the right part of Fig. 6(a)). These packaged components include a filter wheel and filters, a spectrograph, and an Image-Intensified Charge-Coupled Device (ICCD) camera.

#199333 - $15.00 USD Received 14 Oct 2013; revised 21 Feb 2014; accepted 26 Feb 2014; published 1 Apr 2014

Aerosol is pulled into an airtight box (20”L × 16”W × 18”H) at 1.0 Lpm from the aerosol generation subsystem, then focused into a laminar jet of around 500 μm in diameter by a nozzle within the chamber. The nozzle position can be finely adjusted using a μm-resolution micrometer with a motorized actuator that is controlled from the hallway. This controlled micrometer ensures that the nozzle can be adjusted so that the center of the aerosol jet passed through the center of the trigger volume. The trigger volume is approximately 100 μm × 100 μm, and is defined by the intersection of two 5-mW diode-laser beams at 650 nm and 685 nm. The height of the 685-nm laser can also be finely adjusted by a micrometer with a motorized actuator to ensure that the two laser beams are at the same height in the trigger volume. Aerosol particles larger than 1 μm diameter flowing through the trigger volume will be detected from their near-forward elastic scattering, as recorded by two PMTs, i.e., PMT 1 and PMT 2, which have narrow-band interference filters at 650 and 685 nm, respectively.

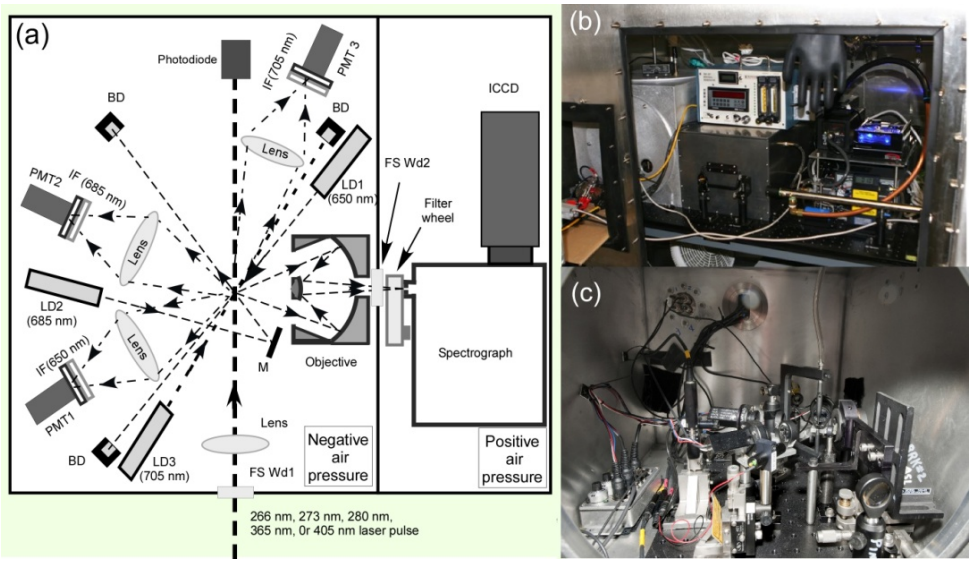

Fig. 6. (a) Schematic diagram of the part of the SPFS that is in the BSL-3 chamber. The diagram emphasizes the optics and optical equipment. Particles flow into the plane of the page through a nozzle at the intersection of the pulsed laser beam (propagating upward in the diagram) with several diode laser beams. Where, BD: beam dump; FS Wd: fused silicon window; IF: interference filter; LD: laser diode; M: mirror; and PMT: photomultiple tube. Photographs of (b) part of the SPFS system within the BSL-3 chamber before the front panel is closed; and (c) part of the SPFS system within the negative airtight box (left part in (a)).

The signals from PMTs 1 and 2 are amplified and fed into two single-channel analyzers (SCA 1 and SCA 2, from Ortec) which operate as discriminators in a window mode (0.1 V – 10.0 V). The PMT pulse voltages must fall between the preset upper and lower voltage levels before the SCA provides an output pulse. The two SCA outputs are fed into a logic AND gate, which produces an output pulse only when the SCAs’ outputs overlap for at least 5 ns. The AND gate output then sends a 500-ns TTL trigger pulse to the laser, ICCD, and data acquisition board. The laser is triggered within ~2 μs of the signal from the AND gate. In 2 μs the particle, with velocity ~10 m/s, travels ~20 μm. In order to compensate for this small vertical displacement, the center of the sample volume is positioned slightly below the position of the trigger volume (the focal volume of the two diode-laser beams). The sample volume is defined by the position of the UV laser beam, and by the focal volume of the reflecting objective of the fluorescence collection optics.

A third diode laser at 705 nm (50 mW) is used in estimating particle size. Its beam is focused about 50 μm below the trigger volume with a spatial profile about 2 mm in width and 200 μm in height. Therefore, any particles passing through the trigger volume also pass

#199333 - $15.00 USD Received 14 Oct 2013; revised 21 Feb 2014; accepted 26 Feb 2014; published 1 Apr 2014

through 705-nm diode laser beam. Because its width (2 mm) is much broader than that of the trigger volume (about 100 μm), particles that pass through the trigger volume should be exposed to a relatively uniform 705-nm intensity. The near forward scattering (10-40 degrees) is detected by PMT3 and used for particle size estimation.

The signals from PMT3 are also amplified, then sent to the data acquisition board (Measurement Computering, MCC/USB-2523), and the digitized outputs are recorded by a computer in the hallway. The trigger signals from PMT 1 and 2 were also used to estimate the position of the detected particle relative to the focus point of the reflective objective. The signals from PMT 1, 2, and 3 are recorded only when the AND gate TTL trigger pulse is generated, and therefore, the trigger, size, and also the fluorescence information are recorded for each particle simultaneously.

When the detected aerosol particle is illuminated by a single pulse of the laser as described above (about 50 μJ/pulse, 1 mm in diameter in the sample volume), the emitted fluorescence is collected by a Schwarzschild reflective objective (Newport 50105-1, numerical aperture 0.4) and dispersed by a spectrograph (Acton 150, grating 300 l/mm, blaze wavelength 300 nm). A long-pass filter set installed in a filter wheel (Princeton filter wheel FA-2448-2) mounted on the front of the spectrograph is used to block the elastic scattering of the laser. Different long-pass glass filters (Newport, colored-glass alternative filter) with cut wavelengths at 280 nm, 295 nm, 295 nm, 380 nm, and 415 nm were used for lasers at 266 nm, 273 nm, 280 nm, 365 nm, and 405 nm, respectively. All filters have about 95% transmission 3 nm above the cut-off wavelength, and have a very steep cut-off at the indicated wavelength. The dispersed spectrum is measured by the ICCD camera (Princeton PI-Max3). The digitalized spectral information is carried by an Ethernet cable to the computer in the hallway.

To protect the equipment within the BSL-3 chamber from being contaminated by agents, so that sensitive and expensive equipment is not ruined by the decontamination procedure we enclosed the filter wheel, spectrograph, and the ICCD detector in a separate airtight box (24”L × 9”W × 15”H), with a positive pressure of 5 mbar above the environment within the BSL-3 chamber (left box in Figs. 6(a) and 6(b)). The other part of the SPFS system, which was exposed to the aerosols, was enclosed in another airtight chamber with a negative pressure of 5 mbar (left box in Figs. 6(a) and 6(b)) relative to the environment. The negative pressure chamber is aspirated at 1 Lpm through an outlet tube concentrically aligned with the inlet nozzle assembly. A piston pump (KNF Neuberger, UN86) draws aerosol through the nozzles and chamber. The pump runs at a speed that draws air at a flow rate of 5 Lpm if there is no restriction. A critical orifice was inserted between the outlet tube and the piston pump to restrict the air flow to 1 Lpm. This forces the air passing through the orifice at subsonic speed to reduce pressure fluctuations caused by the pump within the chamber and to form a uniform aerosol flow from the inlet nozzle. The air is exhausted into the BSL-3 chamber after it is filtered (Parker DFU, grade BX, which block 99.99% of particles above 0.01 μm). The positive-pressure airtight box was supplied by filtered (same filter as above) air at 5 L/min from the BSL-3 chamber with another piston pump, and the air within the box was allowed to leak out after passing through two serially connected- filters, which were arranged to build a 5 mbar pressure step between the box and the BSL-3 chamber.

For recording the LIF spectrum, first the background spectra are measured at the same conditions used to measure the LIF spectra for aerosol particles, except the laser is internally triggered at 10 Hz without the presence of particles. Then the average background spectrum is subtracted from the measured spectrum. The background counts of the ICCD are mainly from the elastic scattering, stray light, and the thermal and read-out noise of the ICCD itself. To ensure that the SPFS system measures the fluorescence spectrum and elastic scattering for one particle at a time, the particle concentration was kept low enough that only one particle at a time enters the interrogation region, except for rare instances of two particles at once.

#199333 - $15.00 USD Received 14 Oct 2013; revised 21 Feb 2014; accepted 26 Feb 2014; published 1 Apr 2014

2.5 Ultraviolet aerodynamic particle sizer

The UV-APS (TSI 3314) was used to provide reference measurements, particularly for the particle concentration and size distribution. It samples the aerosol at 1 Lpm from the aerosol generation and control subsystem. It is provided another 4 Lpm of clean HEPA-filtered air (from the chamber interior) to achieve the total airflow input of 5 Lpm it requires. It measures the aerodynamic particle size and the average fluorescence per particle in each of the size bins excited by a 355-nm laser.

3. Growth and preparation of live agents and surrogates

Bacillus anthracis Ames (BaA), *Yersinia pestis CO92* (Yp), and *Venezuelan equine encephalitis TC83* (VEE), were freshly grown at ECBC. The final concentration of the spores was diluted and counted to be around 1.24×10^9 cfu/mL. Virus was prepared with a concentration of about 10^9 pfu/mL.

The simulant bacteria (*Bacillus thuringiensis var. kurstaki (Btk), Bacillus thuringiengis var. israelensis (Bti), Bacillus atrophaeus* var. *globigii (formerly Bacillus globigii, BG), Bacillus anthracis* Sterne *(BaS), Escherichia coli (E. Coli), Pantoea agglomerans (formerly Erwinia herbicola; Eh), Yersinia rohdei (Yr)*), and the simulant virus (the bacteriophage MS2), were freshly grown at Johns Hopkins University/Applied Physics Laboratory (JHU/APL).

All *Bacillus* spore stocks were resporulated on new sporulation media, and were propagated and sporulated under essentially the same conditions. All newly sporulated and enumerated spore stocks were injected into Modified G medium [21] and grown at 37 °C with aeration of 1 vvm (vessel volume per minute) and agitation rate of 250 rpm for one week, with observation of spore formation by microscopy. Spores were harvested after one week and washed once with 50% ethanol-water and twice with cold, sterile water. The spores were heated to 80 °C for 20 min. The percentage and number of spores were enumerated pre- and post-heating by growth on Trypticase Soy Agar (TSA). Spores were stored at 2-8 °C in sterile water.

P. agglomerans was incubated in nutrient broth with 2% sucrose added at 30 °C for 16-18 h (until turbid). After growth, the sample was centrifuged and pelleted, and the supernatant removed. The pellet was resuspended in 30 mL of phosphate buffered saline (PBS) and enumerated using the BeckmanCoulter Multisizer, prior to aerosolization.

Y. rohdei was incubated at 30 °C for 18 h in brain heart infusion broth. After growth, the *Y. rohdei* culture was washed three times with PBS, each time separating the bacteria from the liquid by centrifugation. The washed Yr was suspended in 30 mL of PBS.

E. coli was incubated at 37 °C for 18 h in EM271 (American Type Culture Collection) broth for 24 h. After growth, the sample was centrifuged and pelleted, and the supernatant removed. The pellet was resuspended in 30 mL of PBS and enumerated using the Beckman Coulter Multisizer (Model MS3; Brea, CA), prior to aerosolization.

MS2 phage was prepared by first growing an *E. coli* culture according to the procedure above. After the culture entered log phase (approximately 3 h), it was seeded with the MS2. This culture was incubated for 24 h at 37 °C. After this second incubation the *E. coli* cells that had not lysed, and at least some of the cell fragments remaining after lysis by MS2, were pelleted by centrifugation. The supernatant containing the MS2, the lysate from the lysed *E. coli* cells, and the spent culture medium was removed. The MS2 concentration was quantified by plaque assay prior to aerosolization.

4. Calibration of the single particle fluorescence spectrometer

4.1 Calibration of wavelengths, relative spectral response, and particle size

Calibration of the wavelengths of the SPFS is accomplished using the elastic scattering peaks of the excitation laser as recorded on the ICCD. The scattering is from particles passing

#199333 - $15.00 USD Received 14 Oct 2013; revised 21 Feb 2014; accepted 26 Feb 2014; published 1 Apr 2014

through the SPFS. Peaks at both the first- and second-order diffraction from the grating are used. The laser wavelengths, in turn, are calibrated by the laser manufacturer and further confirmed by a spectrometer (Ocean Optics, USB4000-XR). For this effort in the BSL-3 laboratory, the SPFS had to be operated remotely for a period of months, even though the excitation wavelength from the laser had to be changed repeatedly, and realigned to illuminate the particles shortly after they exited the nozzle. The laser beam traversed three windows and was reflected by three mirrors on its approximately 2 m path from the laser output to the sample volume inside the SPFS. Therefore the system was designed and constructed so that the trigger system is less sensitive to particle position than in previous efforts [13]. Further, a relatively large sample volume was needed to minimize the chance of the system becoming so misaligned that no data could be obtained. Such an arrangement decreases the accuracy and lowers the resolution to 15 nm for wavelength measurements, due to the variations in particle positions relative to the focal point of the collection optics. Figure 7 illustrates the 273 nm elastic scattering from the first 100 of 1000 1.5 μm PSL spheres. The inset shows some of the extreme traces. The sharpest peaks are from particles nearest the focal point. The others are from various positions away from the focal point in different directions. The sharp peaks help determine the pixel corresponding to the wavelength.

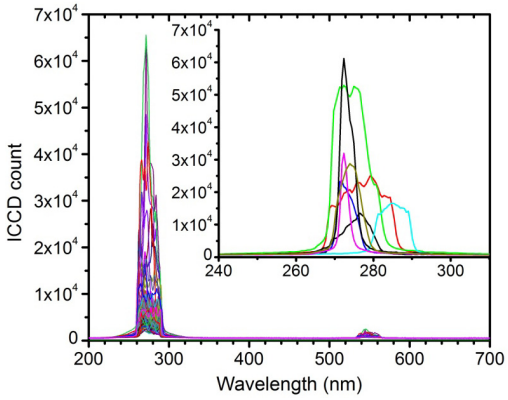

Fig. 7. Recorded elastic scattering from 100 particles of 1.5 μm polystyrene spheres illuminated with a 273-nm laser. The inset shows some examples. The elastic signals are all from 273 nm illumination but were focused to different pixels of the ICCD. These signals appear to be at different wavelengths because the elastically scattered light was focused into the slit of the spectrometer at different angles because the particles were at different positions with respect to the collection optics when they were illuminated.

The relative spectral response for the SPFS system, which includes the collection optics, spectrograph, and ICCD detector, is calibrated based on a NIST-traceable calibration light source from 220 nm to 1050 nm (DH-2000-CAL deuterium tungsten halogen calibration standard, Ocean Optics). The relative response at each wavelength was obtained by comparing the recorded spectrum of the ICCD with the spectrum of the light source provided by the manufacturer. Even though this light source provides the absolute spectral intensity in $\mu W/cm^2/nm$, it is still hard to obtain the absolute spectral response of the system (ICCD counts/per photon at each particular wavelength or pixel), because it is difficult to determine the percentage of the photons emitted from the light source that are collected by the reflecting objective and also exactly where the measured particle is illuminated. Therefore, the absolute response is calibrated using the elastic scattering intensity reaching the collection objective from NIST traceable polystyrene latex (PSL) microspheres with well known sizes (Duke Scientific/Thermo-Fisher). The detailed calibration for absolute spectral response will be described below.

The size of each detected aerosol particle is estimated using the near forward elastic scattering intensity of the 705-nm diode laser which is measured by the corresponding PMT 3

#199333 - $15.00 USD Received 14 Oct 2013; revised 21 Feb 2014; accepted 26 Feb 2014; published 1 Apr 2014

detector (see Fig. 6(a)). It is calibrated using NIST traceable PSL microspheres. Calibration PSL particles are distinguished from surfactant, dust and aggregate particles, by the associated UV-LIF data from the ICCD.

4.2 Motivation for using elastic scattering from polystyrene sphere to calibrate the absolute photon response

The absolute response of the SPFS to light at certain wavelengths is obtained using the elastic scattering from polystyrene latex (PSL) microspheres of known size. The elastic scattering from size calibrated polystyrene spheres can be calculated accurately using Mie theory, and measured by the SPFS system. The scattered photons are collected and recorded using the same optics and ICCD as that which collects and records the fluorescence. Therefore, the absolute response of the SPFS to photons of a particular wavelength (counts/photon) can be determined from the measured ICCD count and the calculated number of scattered photons. This response can be extended to other wavelengths by combing the data at this particular wavelength with the measured relative spectral response. Because this calibration approach uses exactly the same system arrangement as that used for the fluorescence measurement, such a calibration would eliminate the uncertainty caused by the variation of particle position relative to the illuminating laser beam and collection optics. However, differences of densities and shapes between bioparticles and PSL spheres can result in slight differences in particle trajectories and speeds.

4.3 Calculation of the light scattered by a PSL microsphere that reaches the collection optics

To calculate the elastic scattering from PSL microspheres, the refractive index is required at each wavelength. Here, the real part of the refractive index was calculated from:

$$m_r = a + b/\lambda^2 + c/\lambda^4 \quad (1)$$

where a = 1.5663; b = 7850, and c = 3.34 × 10^8 [22]. It is found to be similar to the data estimated from other published literature [e.g. Figure 9 in [23]]. The imaginary part of the refractive index m_i was interpolated from the published measurements [Table 1 in [22]]. The resulting complex refractive indexes were: m = 1.744 + i0.01 at 266 nm; m = 1.732 + i0.005 at 273 nm; m = 1.721 + i0.0004 at 280 nm; m = 1.644 + i0.0 at 365 nm; and m = 1.627 + i0.0 at 405 nm. Based on these data, the scattering reaching the secondary mirror of the reflecting objective was calculated using a modified version of the separation of variables (Mie theory) codes [24]. The calculated differential cross section at 90 degree is illustrated in Fig. 8. Eventually, the average energy per solid angle (sr) that is scattered by particle and reaches the reflecting objective can be obtained by multiplying the cross section (μm^2/sr) with laser fluence (J/μm^2).

4.4 Calibration of the SPFS using the light scattered by PSL microspheres

The calculated average differential scattering cross sections from Fig. 8 are used to calibrate the spectrometer as follows.

Let $S(\lambda_i)$ be a corrected measured spectrum. Here by "corrected" we mean that it has had the average background spectrum subtracted and has been divided by the spectral response of the system as described in subsection 4.1. The average background spectrum is the average of (typically) 1000 spectra measured when the laser fires and the ICCD records the spectrum, when no particles pass through the system. The λ_i include both the emission and scattering wavelengths. $S(\lambda_i)$ is a discrete spectrum. The λ_i are the center wavelengths of the bins. Although the ICCD has 1024 pixels, the spectra are binned into a smaller number of bins to reduce the variability from bin to bin. For the results shown here, the bin size is 5 nm.

Let $S_{p,d,{}^e\lambda}(\lambda_i)$ be a corrected measured spectrum for polystyrene spheres where the subscripts p,d,$^e\lambda$ indicate the material (in this case, p for polystyrene), diameter (d) of the PSL

#199333 - $15.00 USD Received 14 Oct 2013; revised 21 Feb 2014; accepted 26 Feb 2014; published 1 Apr 2014

spheres, and excitation wavelength (°λ). Because the spectrograph input slit width is set to a large value (1.2 mm), the elastic scattering from the narrow-linewidth laser appears over several wavelength bins. For simplicity, and to avoid adding more notation, the signal from all the elastic scattering channels are combined into one channel which we label,

$$S_s(\lambda_s) = \sum S_{p,d,^\circ\lambda}(\lambda_i), \tag{2}$$

over the wavelengths where elastic scattering appears.

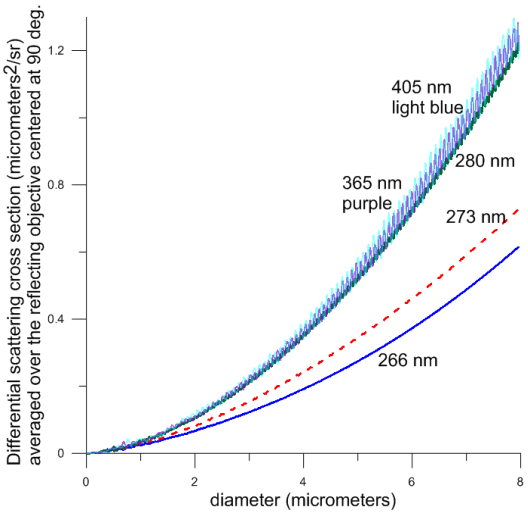

Fig. 8. Calculated average differential scattering cross section (μm²/sr) for polystyrene spheres, averaged over the collection angles (NA = 0.4, between 12 and 23.6 degrees from the axis of the objective) for the Schwarzschild reflecting objective, when the axis of the reflecting objective is centered at the scattering angle of 90 degrees to the laser beam. These average cross sections have been averaged over the particle diameter.

Let $c_s(\theta_c = 90)$ be the differential elastic scattering cross section (μm²/sr) averaged over the aperture of the Schwarzschild objective. Let $c_f(\theta_c = 90, \lambda_i)$ be the differential fluorescence cross section (μm²/sr) for emission within the i^{th} wavelength band, and averaged over the aperture of the Schwarzschild objective. The $c_f(\theta_c = 90, \lambda_i)$ is a discrete spectrum. It can be converted to $c^{nm}_f(\theta_c = 90, \lambda_i)$, the differential fluorescence cross section (μm²/(sr.nm)) by dividing by the number of nm in the discrete wavelength bin.

Let T_a = the average fluence (J/μm²) that illuminates the particles in some region R. Also, assume that T_a does not change between the calibration and measurement runs.

The elastic scattering from the particle that reaches the aperture is: $T_a c_s \Delta\Omega$ (J), where $\Delta\Omega$ is the solid angle subtended by the Schwarzschild objective. Also, the fluorescence from the measured bioparticle that reaches the aperture is: $T_a c_f \Delta\Omega Y$ (J), where Y is the filter transmission. For the calibration using PSL particles, no filter is used, and so for that case Y is omitted.

The amplitudes of the spectra (S_s and S_f) generated within the respective wavelength bands on the spectrograph are then,

$$S_s(\lambda_{i=s}) = K T_a c_s(\lambda_{i=s}) \Delta\Omega G_s \tag{3}$$

for the elastic scattering, and,

$$S_f(\lambda_i) = K T_a c_f(\lambda_i) \Delta\Omega Y G_f \tag{4}$$

#199333 - $15.00 USD Received 14 Oct 2013; revised 21 Feb 2014; accepted 26 Feb 2014; published 1 Apr 2014

for the fluorescence, where K is a constant that relates the energy of the light collected to the amplitude of the spectra S(λ) read by the ICCD. The lower equation is divided by the upper to eliminate the $KT_a \Delta\Omega$. Solving for c_f gives:

$$c_f(\lambda_i) = [S_f(\lambda_i) / Y G_f][c_s(\lambda_{i=s}) G_s / S_s(\lambda_{i=s})] \quad (5)$$

This is the expression used to obtain the $c_f(\lambda_i)$, the main parameter calculated and discussed in the results and discussion. The c_s is calculated. The $S_s(\lambda_{i=s})$ measured and corrected. The G_s is the gain setting for that measurement. $S_f(\lambda_i)$ are recorded by the ICCD and corrected with background subtraction and division by the system response. It is convenient to write Eq. (5) in terms of a calibration factor by which the measured $S_f(\lambda)$ is multiplied, and to divide by 5 nm to so that the final output is in cm^2/nm.sr, i.e.,

$$c^{nm}{}_f(\theta_c = 90, \lambda_i) = C S_f(\lambda_i) \quad (6)$$

where, C, the calibration factor, is given by

$$C = c_s(\lambda_{i=s}) G_s / (S_s(\lambda_{i=s}) 5 Y G_f) \quad (7)$$

For a set of spectra of calibration particles, the $c_s(\lambda_i)$ are calculated for each particle and then averaged, and the $(S_s(\lambda_{i=s})$ are also averaged. It is these averaged values of $c_s(\lambda_i)$ and $S_s(\lambda_{i=s})$ that are used in the above expression for C.

The PSL spheres used for determining C have a size deviation within ± 15%. In the calibration measurements it is not clear how to tell which particles are PSL and which, if any, PSL spheres have a residue from the surfactant in which these PSL spheres are suspended, and which, if any, particles may be primarily surfactant material. Therefore in determining the calibration factor C, we use the forward scattered light from a diode laser at 705 nm (described in Section 5.1 below) to estimate the particle size, and to use for calibration only those particles which have a size within the known size range (approximately ± 15%) of the calibration PSL.

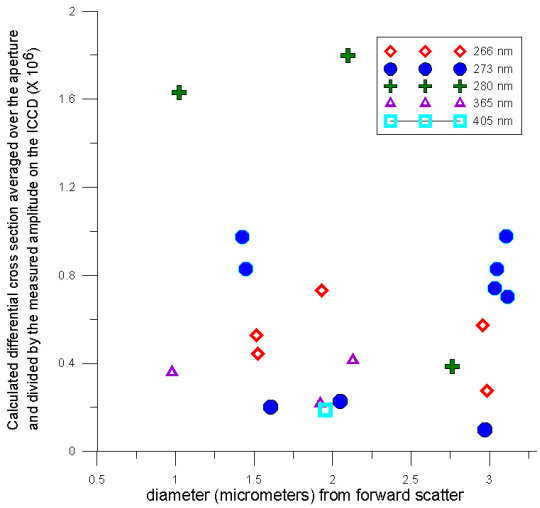

Fig. 9. Calibration factors determined using PSL particles of different sizes. The average values of the cross sections at each wavelength are 0.51 ± 0.17 at 266 nm, 0.62 ± 0.32 at 273 nm, 1.27 ± 0.63 at 280 nm, 0.33 ± 0.10 at 365 nm and 0.19 at 405 nm.

The results for 18 calibration runs are shown in Fig. 9. The final calibration factors C obtained for each wavelength are the averages of the C factors for all the calibration measurements at this wavelength, i.e., the average C factors obtained are 0.51 ± 0.17 at 266 nm, 0.62 ± 0.32 at 273 nm, 1.27 ± 0.63 at 280 nm, 0.33 ± 0.10 at 365 nm and 0.19 at 405 nm.

#199333 - $15.00 USD Received 14 Oct 2013; revised 21 Feb 2014; accepted 26 Feb 2014; published 1 Apr 2014

Because we were unable to measure the fluences (J/cm^2) in the region where the particles are illuminated, and we were unable to obtain an overall average calibration factor.

4.5 Angular dependence of fluorescence emission from particles

Fluorescence cross sections reported previously for bacteria are (so far as we know) presented as if the fluorescence is emitted isotropically. The emission, which is measured in some solid angle typically centered around 90 degrees from the illuminating direction, is multiplied by the ratio of solid angles to obtain the total cross section. For vegetative cells in water, that is probably adequate.

However, the fluorescence emission from molecules in aerosolized microparticle is emitted preferentially in the direction of illumination laser, and the least emission is in the region near 90 degrees [25, 26]. The enhancement of the backward directed fluorescence emission increases as the ratio of the particle's refractive index to that of the surrounding medium (typically air or water) increases. For vegetative cells in aqueous phosphate buffered saline this non-isotropic effect would be very small, because the refractive index difference between the bacteria and the liquid is very small. For spores or dry vegetative bacteria in air the relative refractive index is around 1.5 and 1.44 respectively, and the effect would be significant, and the backward fluorescence at 180 degrees could be several times stronger than that in the 90 degree direction. For dried spores it is calculated to be about 3.5 times stronger [25, 26].

Because most fluorescence-based particle counters (including the SPFS) collect fluorescence centered around 90 degrees from the direction of the laser beam to avoid the forward or backward elastic scattering, the most relevant fluorescence cross section should be an average over an aperture centered at 90 degrees. Therefore, we present the averaged fluorescence cross section determined from the measurement around 90 degrees without considering the angular dependence for fluorescence emission from particle. However, for standoff detection, the relevant cross section for a small-solid-angle detector centered near 180 degrees, the fluorescence cross section (e.g. for *Bacillus* spores) is likely to be about 3 times larger than the cross section given here [26].

5. Results

The system was developed and tested during June 2010-February 2011, and installed and aligned at a BSL-3 facility at ECBC at the beginning of March 2011. The measurements were made from March 21 to April 7, and on May 24 and 26, 2011.

5.1 Size distributions of biological samples

Figure 10 shows typical size distributions of the aerosolized BaS-CLN and Bg samples, 1000 particles measured by the UV-APS, and the SPFS. CLN indicates the "clean" sample that has been washed and centrifuged eight times.

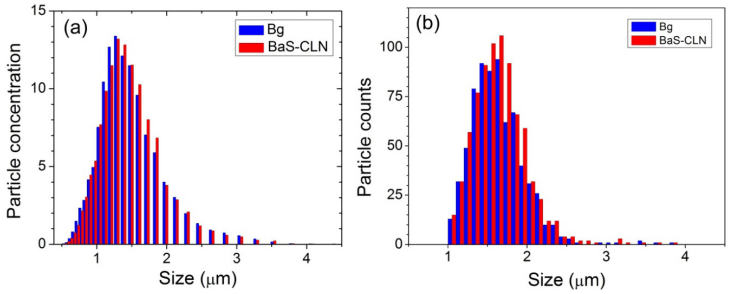

Fig. 10. Typical size distributions of the aerosolized bioaerosol particles in the measurements. (a) Measured by the UV-APS. (b) Measured by the SPFS.

#199333 - $15.00 USD Received 14 Oct 2013; revised 21 Feb 2014; accepted 26 Feb 2014; published 1 Apr 2014

The aerosol particles generated by this system are generally in a log-normal size distribution. The mode size, mean size, and standard deviation mainly depend on the concentration of the agent solution under the same aerosol generation conditions. When the data is fit to a log-normal distribution, the mean size are found to be 1.44 ± 0.27 μm for BaS; 1.42 ± 0.26 μm for BG measured by UV-APS (Fig. 10(a)); 1.62 ± 0.21 μm for BaS; and 1.59 ± 0.21 μm for Bg detected by the SPFS (Fig. 10(b)). All regression-squared are larger than 0.99 in these fits. The UV-APS measures the aerodynamic size of the particles delivered to the system, providing a size-resolved distribution for the particles larger than 0.523 μm. However, the SPFS system does not respond to particles smaller than about 1 μm diameter. The nozzle of the SPFS focuses a higher percentage of the larger (greater than 2 μm) particles into the trigger volume (with its diameter of about 100 μm) than the smaller (less than 2 μm) particles. Therefore, the larger particles have a higher probability of being detected by the SPFS.

5.2 Single-particle spectra

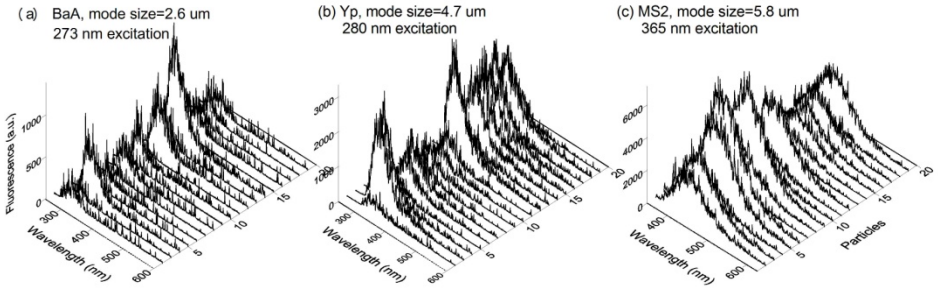

Fig. 11. Typical single particle UV-LIF spectra from different size aerosol particles of BaA, Yp, and MS2 excited by 273 nm, 280 nm, and 365 nm respectively.

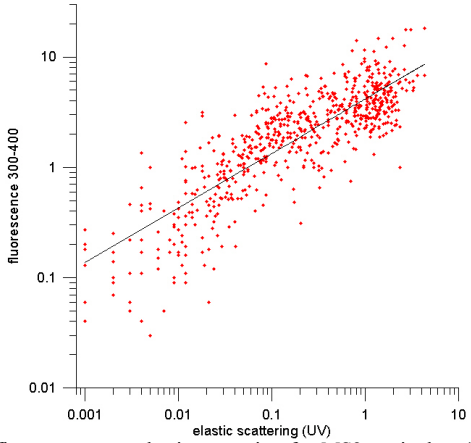

Fig. 12. Measured fluorescence vs elastic scattering for MS2 excited at 405-nm. The best fit line is given by: ln(integrated fluorescence intensity) = 0.518 × ln(elastic scattering intensity) + 1.477.

Figure 11 shows typical single-particle UV-LIF spectra from 20 successive aerosol particles of BaA, Yp, and MS2 excited by 273 nm, 280 nm, and 365 nm with mode diameters 2.6, 4.7 and 5.8 μm, respectively. These spectra have consistent spectral profiles. The differences in fluorescence spectral intensities for different particles are mainly caused by variations in particle sizes, and also the relative position of the particle with respect to the collection optics when it is illuminated. The spectra from the large particles have stronger fluorescence emission with larger apparent SNR (e.g., in Fig. 11(c)). The z-axis is the count of the direct reading from the ICCD. Another cause of variation in amplitude in Fig. 11 is the variation in illumination intensity on the particle, resulting from spatial and shot-to-shot variations of the

#199333 - $15.00 USD Received 14 Oct 2013; revised 21 Feb 2014; accepted 26 Feb 2014; published 1 Apr 2014

incident beam. However, these variations are relatively small (less than 5%). Figures 11(a) and 11(b) show the fluorescence in the 250–600 nm range. Figure 11(c) shows fluorescence in the 350–625 nm range.

5.3 Single-particle fluorescence vs elastic scattering

Because the collected fluorescence intensities from different particles are strongly dependent on particle position relative to the collection optics and on the particle composition there are large variations in the intensities measured for the elastic scattering and fluorescence, as illustrated in Fig. 12. Reasons for this variation are discussed further in Section 6.

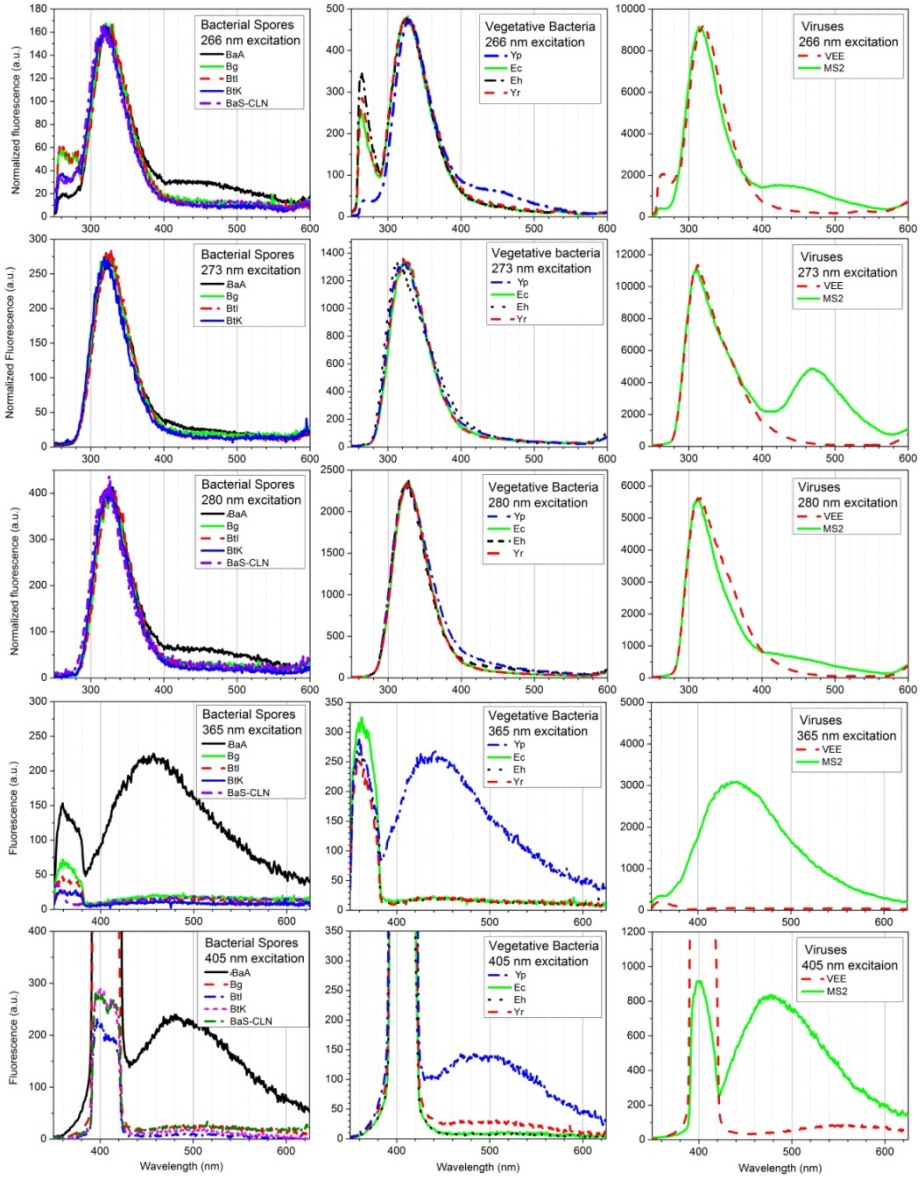

Fig. 13. Averaged UV-LIF spectra of 1000 single aerosol particles from various live agents and surrogates excited at 266 nm, 273 nm, 280 nm, 365 nm, and 405 nm. The peaks around the excitation wavelengths are the leakages of the elastic scattering. The spectra excited by 266 nm, 273 nm, and 280 nm are normalized to the same peak intensities at about 330 nm for easy comparisons of spectral profiles. The spectra excited at 365 nm and 405 nm have not been normalized.

#199333 - $15.00 USD Received 14 Oct 2013; revised 21 Feb 2014; accepted 26 Feb 2014; published 1 Apr 2014

5.4 Averaged fluorescence spectra

Figure 13 shows the averaged UV-LIF spectra of 1000 individual aerosol particles for different measured samples excited at 266, 273, 280, 365, and 405 nm. The sharp peaks around the corresponding wavelengths, particularly at 266 nm (first row), 365 nm (fourth row), and 405 nm (fifth row), are the leakages of elastic scattering, which have not been totally blocked by the corresponding filters. The spectra excited at 266 nm, 273 nm, and 280 nm are adjusted to the same peak intensities for easy spectral profile comparison. However, the spectra excited by light at 365 nm and 405 nm have not been adjusted, other than subtracting the background and applying the spectral response calibration, because the fluorescence from some samples (e.g., BtK) is too weak and too noisy to be adjusted for comparisons of the spectral shapes.

Table 1. Averaged total and peak fluorescence cross sections from about 2000 (range 980 to 3000) particles of various aerosolized live agents and surrogates excited at 5 different wavelengths.

Excitation wavelength (nm)	Name of agent	Fluorescence cross section (10^{-12}cm^2/sr·particle)	Peak flu. cross section (10^{-12}cm^2/sr·nm·particle)	Average particle diam. (μm)
266	BaA	2.62	0.0291	1.66
266	BaS, unwashed	1.08	0.0143	1.47
266	BaS, washed 1x	1.16	0.0161	1.55
266	BaS, clean	0.97	0.014	1.35
266	BG	0.74	0.0099	1.56
266	Bti	0.93	0.0127	1.37
266	Btk	1.75	0.025	1.36
266	Yp	17.94	0.2574	1.89
266	*E.coli*	3.05	0.0486	2.68
266	Eh	2.22	0.0344	2.79
266	Yr	2.45	0.0371	2.76
266	VEE	14.09	0.2217	2.08
266	MS2	43.05	0.5530	2.43
273	BaA	3.59	0.0492	1.96
273	BG	1.11	0.0156	1.66
273	Bti	1.21	0.0182	1.45
273	Btk	1.14	0.0178	1.36
273	Yp	25.87	0.3891	3.38
273	*E. coli*	6.94	0.1101	3.31
273	Eh	5.43	0.0807	3.26
273	Yr	8.00	0.1244	3.32
273	VEE	25.94	0.4401	3.5
273	MS2	80.34	0.8193	3.39
280	BaA	6.09	0.0707	1.95
280	BaS, unwashed	1.05	0.0123	1.63
280	BaS, washed 1x	1.10	0.0144	1.5
280	BaS, clean	1.14	0.0154	1.51
280	BG	1.98	0.0248	1.57
280	Bti	1.90	0.0268	1.57
280	Btk	3.08	0.0448	1.49
280	Yp	24.00	0.3400	2.73
280	*E.coli*	11.66	0.1928	2.19
280	Eh	8.40	0.1355	2.22
280	Yr	14.96	0.2469	2.25
280	VEE	39.21	0.6006	3.27
280	MS2	57.94	0.8344	3.22

#199333 - $15.00 USD Received 14 Oct 2013; revised 21 Feb 2014; accepted 26 Feb 2014; published 1 Apr 2014

365	BaA	1.370	0.0103	1.73
365	BaS, unwashed	0.30	0.0022	1.28
365	BaS, washed 1x	0.21	0.0014	1.19
365	BaS, clean	0.14	0.0009	1.19
365	BG	0.14	0.0008	1.53
365	Bti	0.14	0.0011	1.34
365	Btk	0.09	0.0006	1.3
365	Yp	1.30	0.0098	2.63
365	*E.coli*	0.14	0.0008	2.02
365	Eh	0.12	0.0007	1.99
365	Yr	0.17	0.0010	2.7
365	VEE	0.40	0.0023	3.01
365	MS2	15.44	0.1290	2.33
405	BaA	0.93	0.0071	1.87
405	BaS, unwashed	0.17	0.0011	1.45
405	BaS, washed 1x	0.12	0.0007	1.42
405	BaS, clean	0.11	0.0007	1.36
405	BG	0.13	0.0008	1.69
405	Bti	0.07	0.0005	1.3
405	Btk	0.11	0.0008	1.56
405	Yp	0.60	0.0046	2.94
405	*E. coli*	0.06	0.0005	2.89
405	Eh	0.05	0.0004	3
405	Yr	0.11	0.0008	3.01
405	VEE	0.32	0.0026	2.92
405	MS2	2.98	0.0264	2.95

All samples have strong fluorescence emission in the 280–400 nm range when excited at 266 nm, 273 nm, and 280 nm. The bacterial fluorescence peaks around 320–330 nm. The viral particle fluorescence, which is probably dominated by the fluorescence of the lysate of the Vero cells (in the case of VEE), or *E. coli* cells (in the case of MS2), and some of the spent culture medium in which they were grown, peaks around 310–320 nm. BaA, BaS, Yp, and the MS2 sample, have strong fluorescence emission at 400–600 nm when excited at any of the five wavelengths. This visible emission (400-600 nm) is about 1/5 to ~1/10 of the UV band (280–400 nm) when excited by 266 nm, 273 nm, and 280 nm. This visible band has a peak around 450 nm when excited at 365 nm, and is red-shifted to 475–500 nm when excited at 405 nm. Other samples have little fluorescence emission above 400 nm. But keep in mind that these spectral profiles and intensities could change under different atmospheric environments [e.g., 27].

5.5 Fluorescence cross sections

Table 1 summarizes the total fluorescence cross sections averaged from about 1000 to 3000 particles, but most commonly from about 2000 particles of various aerosolized live agents and surrogates excited by 266 nm, 273 nm, 280 nm, 365 nm, and 405 nm lasers. Note that each data row is from a different group of aerosol particles with a different size distribution and mean size value. Even slightly different aerosol generation conditions may result in different fluorescence cross sections. This study is trying to determine if the live agents have the same optical properties as simulants, and/or which simulant has the closest properties to the corresponding agent for fluorescence-based bioaerosol detection system. We hope these data can aid in the design of bioaerosol detection systems, and in choosing the most suitable simulants for system development and field testing. For bacterial spores, prepared under the conditions in this study, Btk has optical properties similar to BaA, based on the particle size and total fluorescence intensity when excited at 266-nm [e.g 5], 273 nm, or 280 nm.

#199333 - $15.00 USD Received 14 Oct 2013; revised 21 Feb 2014; accepted 26 Feb 2014; published 1 Apr 2014

For vegetative bacteria, the simulants *E. coli*, Eh, and Yr tested here all have smaller fluorescence cross sections than Yp, particularly in the visible range. It appears that this difference is because the Yp was suspended in distilled water before aerosolization while the other vegetative bacteria were resuspended in PBS, which is about 1% solids by weight. The droplet size generated by the Sono-Tek had a size distribution that peaked at about 18 μm diameter, which at 1% solids would dry to a particle with a diameter of $(18^3 \times 0.01)^{1/3} = 3.9$ μm. The MS2 preparation used here (which is predominantly the lysate from E. coli) is not a good simulant for the preparation of VEE used here (which is predominantly the lysate from Vero cells). In our preparations, the viruses were a small enough fraction of the particle that their contribution to the fluorescence is very likely small. The fluorescent molecules in purified MS2 or VEE should be mainly from tryptophan and tyrosine.

5.6 Fluorescence cross sections: Comparison of our results with other measured values

Several research groups have measured fluorescence cross sections for bacterial spores and vegetative cells (see Table 2 below [17, 28–35]). Our values for *Bacillus* are in bold in the last row of the table. For example, Faris et al [28, 29] reported spectra for aerosolized *B. subtilis*, with peak 270-nm excited fluorescence cross sections of 1.5×10^{-14} cm^2/(nm sr spore) for wet aerosol and 0.3×10^{-14} cm^2/(nm sr spore) for dry aerosol (see the bottom two panels in Fig. 8 of [28]). From the spectra presented by Faris *et al.*, we can estimate that their total fluorescence cross sections for emission in the wavelength range from 290 and 390 nm is about 1×10^{-12} cm^2/(sr spore) for wet aerosol and 0.2×10^{-12} cm^2/(sr spore) for dry aerosol. Different spore sizes were used by different groups in calculating the cross sections. For example, Atkins *et al.* [33] used spores measured as 1μm × 0.5μm; Faris *et al.* [28, 29] used 1.25 μm × 0.75 μm; and Manninen *et al.* [17] used 1.1 μm × 0.48 μm (values from the literature). Carrera *et al.* [35] found the size of *B. subtilis* spores to be 1.07 μm × 0.48 μm using electron microscopy. Comparisons among the values in Table 2 are complicated by the variations in preparation methods and the differences and uncertainties in sizes. The values reported in this paper, given in the last row of the table, appear to be within the range of values reported by the other researchers cited in the table.

6. Discussion

6.1 Factors affecting the accuracy of the cross sections determined from the measurements

Because of the many difficulties in working in the BSL-3 laboratory, and our inability to obtain as many replications as desired, we did not calculate the error bars for the measured cross sections in Tables 1 and 2, even though the concept for the calibration scheme is relatively straightforward in principle. As far as we know, none of the reports of the measured fluorescence cross sections from aerosolized bacteria include error bars for the cross sections, although Faris *et al.* [29] estimated that the absolute accuracy of their measurements was a factor of two, limited mainly by the uncertainty in particle numbers [29]. Kunnil *et al.* listed standard deviations for the absorption cross sections and quantum efficiencies of the particles on a quartz slide they placed in a cuvette inside a spectrograph [31], where the sources of error are in some ways easier to estimate. There are, however, additional questions raised in different calibration methods, e.g., in the case of Kunnil *et al.*, how does the particle being on a surface affect the measured absorption cross section and fluorescence cross section? Here we discuss some of the sources of error in calibrating and measuring fluorescence cross sections, with an emphasis on our setup in the BSL-3 laboratory.

#199333 - $15.00 USD Received 14 Oct 2013; revised 21 Feb 2014; accepted 26 Feb 2014; published 1 Apr 2014

Table 2. Fluorescence cross sections measured by several groups. In some cases the numbers shown were estimated from Figs or from other reported numbers.

Researcher(s)	Sample	Fluorescence cross section	Peak Fluorescence Cross Section	Excitation wavelength	State and size of sample
Faris *et al.* 1997, Fig. 8 [29]	*B. subtilis* spores	Wet: $1X10^{-12}$ cm^2/(sr·particle) estimated from spectrum in Fig. 8, Dry: $0.2X10^{-12}$ cm^2/(sr·particle)(est)	1.5 X 10^{-14} cm^2/(nm sr spore) for wet aerosol; 0.3 X 10^{-14} cm^2/(nm sr spore) for dry aerosol	270 nm	Aerosol
Manninen *et al.*, 2009, Fig. 2 [17]	*B thuringiensis* spores in dry PBS	0.4 X 10^{-12} cm^2/(sr·particle) est. from number at right	0.6 X 10^{-14} cm^2/(nm sr spore) for aerosol (cross section divided by 4π sr)	280 nm	Aerosol
Sivaprakasam *et al.*, 2004 [30]	*B. globigii* (BG) spores, Dugway, washed	0.7 X 10^{-12} cm^2/(sr·particle)		266 nm	Aerosol 1 μm Converted with fluor-elastic assumption
Kunnil *et al.*, 2005 [31]	*B. subtilis* spores, washed	0.65 X 10^{-12} cm^2/(sr·particle)	$1.1X10^{-14}$ cm^2/(sr·nm·particle) est. from number at left	280 nm	Dried spores on quartz slide 1.1μmx.48μm
Stephens, 1999 [32]	*B. globigii* spores	0.3 X 10^{-12} cm^2/(sr·particle)	0.8 X 10^{-14} cm^2/(nm sr particle)	270-290 nm from lamp	Aerosol held in electrodynamic trap
					Broad dist.
					Avg > 1 μm
Atkins *et al.* 2007 [33]	*B. globigii* spores	0.03 X 10^{-12} cm^2/(sr·particle)	0.08 X 10^{-14} cm^2/(nm sr spore)	266 nm	Dilute aqueous suspension
					1μm x 0.5μm
Weichert *et al.* 2002 [34]	*M. luteus*	3 X 10^{-12} cm^2/(sr·particle)	8 X 10^{-14} cm^2/(nm sr particle) (cross section divided by 4π sr)	280 nm	Aerosol dry
					1 μm
This paper	**Bacillus spores in Table 1.**	**0.91–3.2 X 10^{-12}**	**1.2-3.6 X 10^{-14}**	**266 nm**	**1.35-1.66 μm**
		1.1-3.6 X 10^{-12}	**1.6-5.0 X 10^{-14}**	**273 nm**	**1.36-1.96 μm**
		0.54-3.0 X 10^{-12} cm^2/(sr·particle)	**0.06-3.5 X 10^{-14} cm^2/(nm sr particle)**	**280 nm**	**1.49-1.95 μm avg. diameter**

The system calibration requires placing a *calibrated light source in the same region as that occupied by the particles when their fluorescence is measured*. Because high NA collection optics was used, and the illumination source was focused tightly, the position dependence of the particles is more severe than in systems that collect less of the light. Raman emission from air has been used for system calibration by Faris *et al.* [28]. In their measurements particles flow through a cylindrical volume with a size of 3.8 mm in diameter and 6 mm in length. It appears to us that their calibration approach must assume that the Raman signal from the air and the fluorescence from the particles are in the same volume, and that the particles are uniformly distributed throughout this volume (as the air molecules are). In our work and the single-particle work of Sivaprakasam *et al.* [30], the calibrated light source is the elastic scattering by polystyrene spheres of known size. Key assumptions in such a calibration are: 1) the calibration spheres reaching the sample volume of the LIF system are single spheres of known size. 2) The complex refractive index of the calibration spheres is known adequately. 3) The sampled calibration spheres and the sampled particles have the same spatial distribution with respect to the collection volume. Although the elastic scattering from the calibration spheres and the fluorescence from the sampled particles have different angular distributions, the position dependence of the measured elastic scattering and fluorescence should average out. Other factors affecting the accuracy of cross section measurements are as follows.

6.2 Variations in calibration values

As shown in Fig. 9, the average values of the calibration factors C at each wavelength have large variations. The ratio of the highest to the lowest values of the calibration factors C for the fluorescence are approximately, 3 × at 266 nm, 16 × at 273 nm, 4.6 × at 280 nm, and 2 × at 365 nm, and only one measurement is done for 405 nm. Such a large variation in the calibration factor in different measurements is a key factor that makes it hard to estimate the

#199333 - $15.00 USD Received 14 Oct 2013; revised 21 Feb 2014; accepted 26 Feb 2014; published 1 Apr 2014

accuracy of the absolute cross sections. The residue of surfactant attached to the PSL particle after the water dries (this surfactant is in the solution as sold by the manufacturer) may be a contributing factor to this variation, possibly because the differing diameters of the initially generated droplets could result in particles with differing amounts of surfactant on them.

In light of the above, it is worth noting that in our measurements, the peak intensity difference between two 1000-shot averages from two sequential runs (within 10 minutes) of the same sample at one excitation wavelength was typically within 15%. Such a relatively small difference indicates that the SPFS system and alignment is relatively stable, and the size distribution did not change tremendously during a typical particle generation period also.

6.3 Variations in the particle position relative to the collection optics can cause variations in individual spectra

To obtain an adequate fluorescence spectral signal from a single 1-μm particle, the emission must be collected over a large solid angle, i.e., large numerical aperture (NA) collection optics is required, and also over a large wavelength range (280 nm to 650 nm). In order to avoid chromatic aberration over this large wavelength range, reflective optics is the best selection. To satisfy these requirements, a 0.4 NA Schwarzschild reflecting objective was used to collect the fluorescence and scattered UV light. However, high NA optics has some drawbacks, e.g., the resulting small depth of field causes high sensitivity to the positions of the fluorescent particles. Consequently, a small displacement of the particle from the focal point results in a magnified and displaced image of the particle at the entrance of the spectrometer (15 × magnification for the objective used). In order to provide an adequate spectral resolution, the spectrometer slit width was set to 1.2 mm. Therefore, some of the fluorescence from the particle, initially "collected" by the Schwarzschild lens could be lost within the reflecting objective or blocked by the input slit. Also, the two crossed-diode lasers used to define the "trigger region," could not be focused as tightly as in some previous versions of the SPFS. This trigger volume is relatively large (approximately 100 μm × 100 μm) to make sure particles can be detected with a reasonable sample rate even in this system which must be remotely operated for a period of months, and with changes of incident wavelength, etc. Given the large variation in collection efficiency from particles at different positions with respect to the collection optics, and the problems envisioned for a laser in a hallway illuminating a small region on a different optical platform, the variations in the intensities measured for the elastic scattering and fluorescence, as illustrated in Fig. 12, are reasonable good.

6.4 Particle-size measurement: uncertainties and effects

The size of each measured particle is estimated from the forward elastic scattering from an 705-nm diode laser beam. The beam is expanded to 2 mm horizontally, which is much wider than the trigger area around 100 μm, in an attempt to keep the incident intensity on the particle relatively uniform. The scattering is collected with a lens and measured with a photomultiplier tube. When the calibration particles passing through this beam are uniform polystyrene spheres of a diameter within the distribution specified by the manufacturer, the voltage recorded by the PMT was relatively uniform and in good agreement with their aerodynamic sizes (measured using a TSI 3321 aerosdynamic particle sizer). The uncertainty caused by this size measurement is far smaller than the two above factors as shown in Fig. 12.

6.5 Possibility of contamination by particles from a prior run

Contamination by particles from the previous run (possibly by attaching to a surface and then vibrating off at a later time) is minimized by the monitoring of UV-APS and confirmed by the subsequent data analysis. Given the time constraints for these tests, some contamination from run to run is probably unavoidable. However, between each run the aerosol concentration, as measured by the UV-APS, was allowed to return to essentially zero prior to the start of the

#199333 - $15.00 USD Received 14 Oct 2013; revised 21 Feb 2014; accepted 26 Feb 2014; published 1 Apr 2014

next run. No obvious foreign spectrum was observed with 1000 spectra for each run, which means that this uncertainty should be negligible, less than 1/1000.

6.6 Uncertainties in the refractive index of the calibration spheres

Errors caused by the use of an incorrect refractive index are probably significant only for the imaginary component of the refractive index. Because the imaginary component of the refractive index is so low at 365 nm and 405 nm, the error from calculated scattering at these wavelengths should be within a few percent, even at 280 nm. Therefore, these scattering values are close enough to the results for non-absorbing spheres that even a large (e.g. 50%) increase in the imaginary component of m_i is not likely to be important relative to the other sources of error in this study. Considering the differences among different polystyrenes with various extents of cross-linking and other factors, the uncertainty caused by the imaginary part of the refractive index at 266 nm and 273 nm is sufficiently small that we interpolated from the literatures as indicated in section 3.4.

6.7 Variability in preparations of biological materials

There are variations in the preparations of agents and simulants even when much care is taken to make the materials as similar as possible. The residue of growth materials and buffer solutions [36], and the amount of water remaining in the aerosol particles after "drying" all affect the fluorescence cross section of the particle. When the slurry of an agent or surrogate is aerosolized into dried particles, the percentages of residue of growth materials or cell fragments may be different from one particle to the next, and the fluorescence intensity may be different, and so these variations may contribute to the variations in fluorescence and scattering as shown in Fig. 12. In experiments such as those described here, where some of the samples are stored for 1 to 2 months, the properties of the samples may change with duration of storage. For example, the measurement of MS2 at 273 nm was done later than the other wavelengths. The sample had been stored in refrigerator for more than 2 months. Changes during storage may have contributed to the relatively stronger fluorescence emission at visible wavelengths seen in Fig. 13.

7. Final remarks

This paper describes the development of a system for measuring the fluorescence cross sections (total and spectrally resolved) of live agents in a BSL-3 facility, and presents the fluorescence cross sections of live agents and stimulants measured with this system. As far as we know these are the first measurements of fluorescence cross sections of live agents which require a BSL-3 capability for aerosolization, and this is also the first system capable of making such measurements. Because of the decontamination requirements and the considerable expense of these instruments which could be destroyed by decontamination procedures, the tunable pulsed UV laser system, and most of the controlling and recording equipments were kept outside of the BSL-3 room. Multiple levels of negative pressure, separated by windows/walls (and other barriers) were used to confine all agents within the BSL-3 chamber. The special requirements for this BSL-3 effort, and how we dealt with them for this setup in a BSL-3 facility, may be useful to other researchers working with aerosolized BSL-3 agents.

Finally, although the applications of fluorescence measurements emphasized here have been in bioaerosol point sensors using single-photon-excitation, the results could also be useful in lidar detection of fluorescent bioaerosols using single-photon [37, 38] and multiphoton [39, 40] excitation. There is also interest in coherent-control and multiphoton-excited fluorescence-based point sensors [40].

#199333 - $15.00 USD Received 14 Oct 2013; revised 21 Feb 2014; accepted 26 Feb 2014; published 1 Apr 2014